# Rotational Tunneling in Methyl Iodide ($CH_3I$)

An experiment on the High-Flux Backscattering Spectrometer

NIST Center for Neutron Research
Summer School on Methods and Applications of Neutron Spectroscopy


**Abstract**

We will use high-resolution inelastic neutron spectroscopy to examine the temperature dependence of the rotational tunnel splitting of the librational ground state of *methyl iodide* (also known as iodomethane, $CH_3I$), a textbook example of a symmetric quantum top. The goal of this hands-on measurement is to gain an understanding and appreciation of the backscattering technique, get practical experience in obtaining low temperature inelastic neutron scattering data, and reduce and interpret a set of these data.

## Introduction

Methyl iodide is a simple example of a quantum rigid rotor and, as a result, exhibits quantized rotational energy levels. Such rotations take place primarily about the axis aligned with the I and C atoms (see figure 1) and can be measured directly with inelastic neutron scattering. The rotation of the methyl group is detected via scattering of neutrons from the hydrogen atoms. It turns out that hydrogen has an extremely large neutron scattering cross-section, dwarfing the cross-section of carbon by a factor of 15 and iodine by more than 20. An experiment involving scattering from a hydrogenous material like a methyl group yields many scattering events in a short period of time, thus making it ideal to study here.

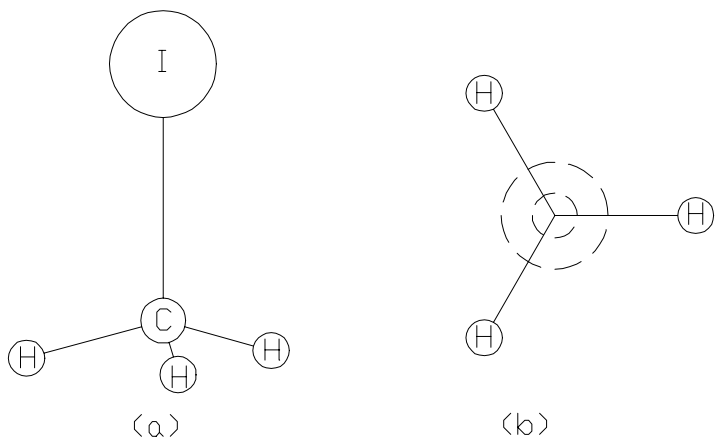


**Figure 1** The $CH_3I$ molecule, (a) side view and (b) view along I-C axis.

In the solid phase the $CH_3I$ molecule is not a free rotor but rather is confined in a potential well. The existence and characteristics of the potential well are a consequence of the molecule's local environment and the motion of the molecule is a direct consequence of this confining potential. Since inelastic neutron scattering probes the motion of the molecules (actually the H atoms in the molecules) then we should be able to extract information about the confining potential from the neutron scattering data.

This interesting molecular system exhibits dynamics on a number of energy scales and we will be probing the extremely low-energy dynamics. In this measurement we will explore the effects of temperature on the very low-energy transitions associated with a type of motion known as *rotational tunneling*. As will be discussed in the theory section, these are the result of splitting *librational* (torsional oscillation) states. In short, rotational tunneling is a term which describes the motion of the H atoms in the molecule as they tunnel through a potential barrier. This *classically forbidden* motion is akin to you walking unimpeded **through** one of the concrete shields surrounding the neutron guides.

At various points throughout the text we will pose a number of questions delimited from the rest of the text with boxes. These are meant to arouse your curiosity (italicized) as well as ensure that you have learned some of the basic ideas and details of this measurement (not italicized). Some of them can be answered based on information presented in this report while others you will have to find out from us. We begin with the following question:

| |
|---|
| Q: *Do you expect the transition energies associated with libration to be higher or lower than those associated with rotational tunneling?* |

**Sample and Sample Environment Details**

Methyl iodide is a liquid at room temperature and solidifies at –66.5$^{o}$C. A small amount of the liquid has been placed into an annular aluminum sample can at room temperature. The annular geometry was selected to minimize the amount of corrections necessary in the data reduction. If the sample is thick and absorbing then some of the neutrons get absorbed. This *self-shielding* depends both on the absorption cross-section of the sample as well as the geometry. For an annular geometry where the neutron sees only a thin portion of the sample, the corrections are negligible. Another concern when determining sample design is minimization of *multiple scattering*. In an ideal neutron scattering measurement we would like for the neutron to scatter once in the sample before reaching the detector. In practice the neutrons can undergo multiple scattering events within the sample and/or are absorbed by the sample, the number of such events increasing with the thickness of the sample illuminated by the beam. One often used rule-of-thumb is to design a sample geometry where 90% of the incident neutrons are transmitted in the forward direction. This is a good compromise between signal and the effects of multiple scattering. A sample with such a design is usually referred to as a *10% scatterer*. Using the known scattering and absorption cross-sections for $CH_3I$ and the geometry one can calculate the desired thickness. For methyl iodide in an annular cell the approximate thickness for 90% transmission in the forward direction is calculated to be 0.13 mm. The annular cell we are using provides a sample thickness of about 0.125 mm.

| |
|---|
| Q: How many times does the beam go through the sample before reaching the detectors? |

This answer to the question posed above can have important consequences for your experiment. If the beam passes through the sample twice (for instance) and the sample has an appreciable neutron absorption cross-section then the intensity at the detectors will be lower than if the beam had only passed once through the sample. Additionally a beam which passes twice through a strongly scattering sample can produce an energy-dependent background.

The sample can has been placed on the end of a sample stick which is in a top-loading orange flow cryostat capable of reaching temperatures as low as 1.4 K. The measurements performed here will span 5 K up to 40 K. The orange cryostat operates on

the basic principle of a heat exchanger (with cold helium flowing through it) in thermal contact with the sample well (which is in thermal contact with the sample stick), thus providing the cooling power. The cryostat contains two reservoirs: a liquid He reservoir surrounding the sample well and a liquid $N_2$ reservoir providing a thermal shield between the He reservoir and room temperature. Periodic replenishment of both reservoirs is necessary for sustained operation of the cryostat. For an experiment like the one being performed here the experimentalist should expect to have to fill each reservoir daily.

## Spectrometer and Data Reduction Details

The HFBS spectrometer is configured in an *inverse scattering geometry*. This means that the energy of the neutron incident on the sample is varied while the final energy of the neutrons reaching the detectors is fixed.

The general principle of operation of HFBS was presented in a lecture so the details will not be repeated here. A summary of the basic principles are as follows:

1. A "white" beam of neutrons back-reflects from the doppler monochromator thus selecting out particular neutron energies, $E_i$, dependent upon the speed of the monochromator when reflected.
2. The reflected neutrons scatter from the sample.
3. Only neutrons with a particular scattered energy, $E_f$, reflect from the analyzer array into the detectors. The energy transfer to the sample is defined as $E=E_i-E_f$.
4. Neutrons scattered from the sample in a particular direction back-reflect from particular analyzers in one of the 16 detectors. This provides the scattering angle, $2\theta$.

| |
|---|
| Q: What is the energy range of the neutrons incident on the sample, $E_i$? What is the fixed final energy of the neutrons reaching the detectors, $E_f$? |

Given the scattering angle, $2\theta$, and energy transfer, E, we may calculate the magnitude of the momentum transfer delivered to the sample, Q. Kinematical arguments lead to the following relationship between $2\theta$, E, $E_i$, and Q:

$$\frac{\hbar^2 Q^2}{2m_n} = E_i - E - 2\sqrt{E_i\left(E_i - E\right)}\cos 2\theta \qquad (1)$$

where $m_n$ is the mass of the neutron.

The data acquisition system records the number of detector counts as a function of initial neutron velocity, $v_i$, where $v_i$ is related to the instantaneous monochromator velocity, $v_m$, and the Bragg velocity of the neutrons with wavelength 6.27 Å, $v_B$, via $v_i=v_B+v_m$. The energy transfer to the sample,

$$E = 2E_B\left(\frac{v_m}{v_B}\right) + E_B\left(\frac{v_m}{v_B}\right)^2, \tag{2}$$

where $E_B$ is the Bragg energy of neutrons with wavelength 6.27 Å, is calculated and written to the raw data file. Note that the motion of the monochromator is time-dependent allowing the variation of $E_i$ necessary to an inverse geometry spectrometer. The raw data measured is recorded as $N(2\theta_j,E_k)=N_{jk}$, the number of neutrons detected in detector j (at scattering angle corresponding to $2\theta_j$) with an energy transfer to sample of $E_k$.

As discussed in the lectures, the quantity which reflects the dynamics of the scattering system most directly is S(Q,E), the dynamic structure function. What we measure, $N_{jk}$, is closely related to the partial differential cross-section, $\frac{d^2\sigma}{d\Omega dE}$. This can be written in terms of the various instrument-dependent parameters and the number of counts received in the detectors,

$$\left.\frac{d^2\sigma}{d\Omega dE}\right|_{j,k} = \frac{N_{j,k}}{\eta(E_f)}\frac{A\eta(FC)}{N(FC)}\gamma_j\frac{1}{\rho_N V}\frac{1}{\Delta\Omega_j}\frac{1}{\Delta E}, \tag{3}$$

where

| | |
|---|---|
| $\eta(E_f)$: | efficiency of a $^3$He detector at the fixed final energy, $E_f$, of the spectrometer |
| A: | area of incident beam |
| $\eta(FC)$: | efficiency of beam monitor |
| N(FC): | total number of counts received in the beam monitor |
| $\gamma_j$: | efficiency correction factor for detector j |
| $\rho_N$: | number density of scatterers in the sample |
| V: | volume of sample illuminated by the beam |
| $\Delta E$: | energy channel width |
| $\Delta\Omega_j$: | solid angle subtended by detector |

We can obtain the dynamic structure function [1], S(Q,E), using the first Born approximation (i.e. a single scattering event dominates the response of the scattering system) via

$$S(Q,E) = \frac{4\pi}{\sigma\hbar}\frac{k_i}{k_f}\frac{d^2\sigma}{d\Omega dE}, \tag{4}$$

where

| | |
|---|---|
| $\sigma$: | scattering cross-section |

| | |
|---|---|
| $\hbar$: | Planck's constant |
| $k_i$: | incident neutron wavevector |
| $k_f$: | final neutron wavevector |

Note that for a sample in thermal equilibrium the *detailed balance condition* is satisfied,

$$S(Q,-E) = e^{-\frac{E}{kT}} S(Q,E), \tag{5}$$

where E is the sample energy gain [1]. This condition is a way of saying that it is more likely that a sample will give energy to the neutron when the temperature is higher rather than lower.

## Theory

In a simplified picture of solid $CH_3I$, an individual molecule can be viewed as having a fixed orientation [2]. This is equivalent to saying that the hydrogen atoms, i.e. protons, are on fixed *labeled* sites. Since the protons are fermions (spin ½), there are three (energetically) equivalent orientations, $|123\rangle, |231\rangle, |312\rangle$, known as *pocket states*.

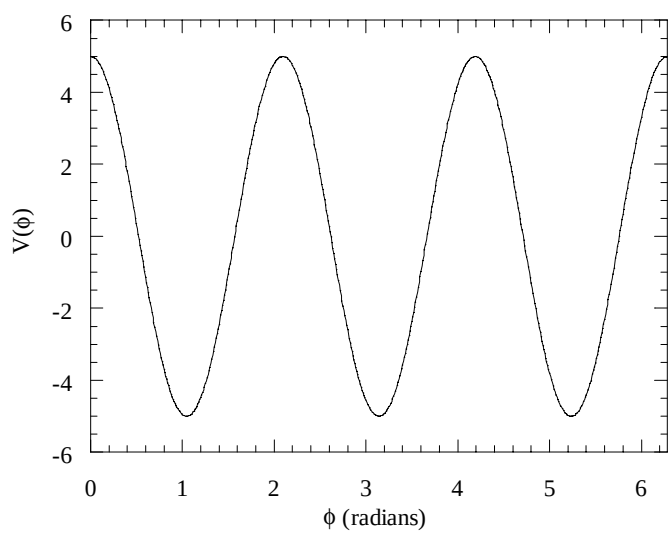


**Figure 2** Simplified three-fold rotational potential for $CH_3I$.

This degeneracy can be conveniently written in terms of a three-fold potential which is expressed approximately as $V(\phi) = A\cos(3\phi+\alpha)$ where the angle $\phi$ describes the angular orientation of the molecule about an axis parallel to the I-C axis (figure 2) and $\alpha$ is a phase. For very strong potential values we approach the case discussed in the previous paragraph where the hydrogen atoms are essentially fixed. In a one-dimensional picture such as this there are two types of motion. The first type of motion is a periodic oscillation within the potential well known as *libration*. The other has to do with the

pocket states. Decreasing the potential strength removes the degeneracy of the equivalent pocket states thus splitting the energy levels so that transitions between the pocket states now involves an energy transfer. This phenomenon is known as *tunnel splitting*. The magnitudes of transitions between librational energy levels are on the order of 10 meV whereas those for tunnel splitting can vary between 1 to 100 μeV at least for splitting of the ground librational state.

The usual starting point for an analysis of the quantum mechanics of the methyl groups is the time-independent Schrödinger equation, $H\Psi = E\Psi$. In one dimension the Hamiltonian for a rotating methyl group is expressed as

$$H = -\frac{\hbar^2}{2I}\frac{\partial^2}{\partial\phi^2} + V(\phi) \tag{6}$$

where $I = 5.3 \times 10^{-47}$ kg m$^2$ for $CH_3$ [3] and $V(\phi) = \frac{V_3}{2}(1 - \cos 3\phi)$. Solution of equation (6) can be carried out numerically using the basis functions for free rotors ($V_3 = 0$),

$$\psi_J(\phi) = A_J \exp(iJ\phi). \tag{7}$$

In the case when the potential is zero the energy levels are given simply by

$$E_J = \frac{\hbar^2 J^2}{2I}, \quad J = 0, \pm 1, \pm 2, \ldots \tag{8}$$

Numerical evaluation of Hamiltonian (6) with the basis functions (7) results in the energy levels depicted in figure 3. Those of you who are interested can find the details of the calculation of the energy levels for the rotor in a three-fold potential in appendix A.

There are a number of notable features in figure 3. First the energy levels at very small values of $V_3$ are spaced according to the free rotor values, given by equation (8). As the strength of the potential increases, some of the branches split apart such as the J=3 and J=6 levels. At high values of $V_3$ some of the separate free rotor energy levels are merged while others are appearing to merge. In particular the J=0 and J=1 levels appear to merge together while the J=3 branch has split and its upper branch seems to merge with the J=2 level. At very high values of $V_3$ (higher than those displayed in figure 3) many such mergers take place for the higher J levels.

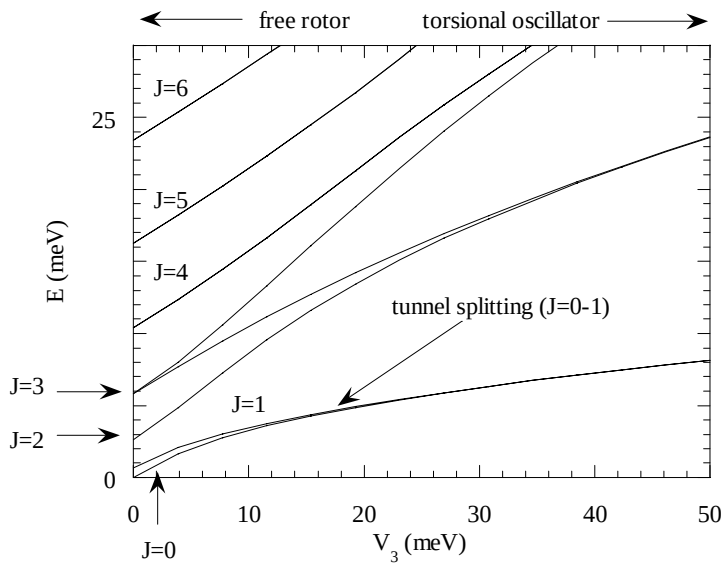


**Figure 3** Energy levels of the rigid rotor as a function of potential strength. The free rotor quantum numbers are listed as well.

The ground state tunneling transition is designated as the transition between the J=0 and J=1 states. The energy for such a transition (the difference in energy between the two levels) is displayed in figure 4 for a broad range of potential strengths. The inset illustrates the tunneling transition energy over a smaller potential strength range.

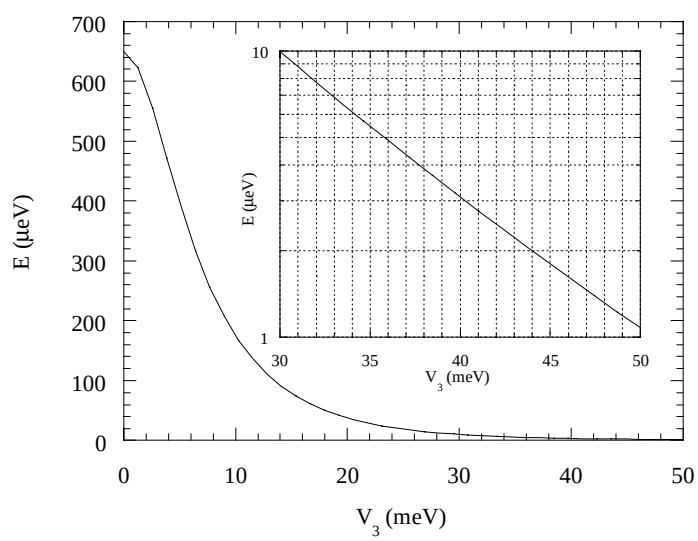


**Figure 4** Energy for the J = 0→1 transition. Inset is a semilog plot illustrating the approximate exponential dependence of the transition energy with potential.

## Data Analysis

A typical raw data scan taken on HFBS is shown in figure 5. There are a number of features in the data. The central peak is the elastic scattering from the sample. The two satellite peaks which are the inelastic scattering are the tunneling peaks.

| |
|---|
| Q: Do the intensities of the inelastic peaks satisfy detailed balance? Is this system necessarily in thermal equilibrium? |

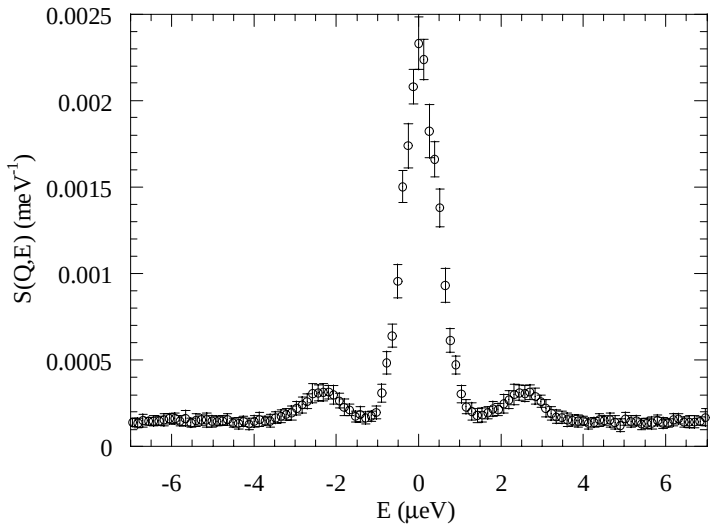


**Figure 5** Backscattering data of $CH_3I$ taken on HFBS at 5 K.

| |
|---|
| Q: What is your estimate of $V_3$ based on the data in figure 5 and the model we have selected? |

The effects of deuteration have been studied with this system as well [4]. Since the nuclei in the methyl group are now composed of a proton and neutron, we would expect that the moment of inertia of the rotor to be doubled. The calculation shown in figure 4 has been repeated with such a modification to the moment of inertia and the transition from the $J=0\rightarrow1$ states are displayed over a similar range in figure 6.

| |
|---|
| Q: If we were to measure $CD_3I$ rather than $CH_3I$ do you think that we'd be able to observe the tunnel splitting with this spectrometer? Assume that the potential strength does not change from your estimate in the previous question. |

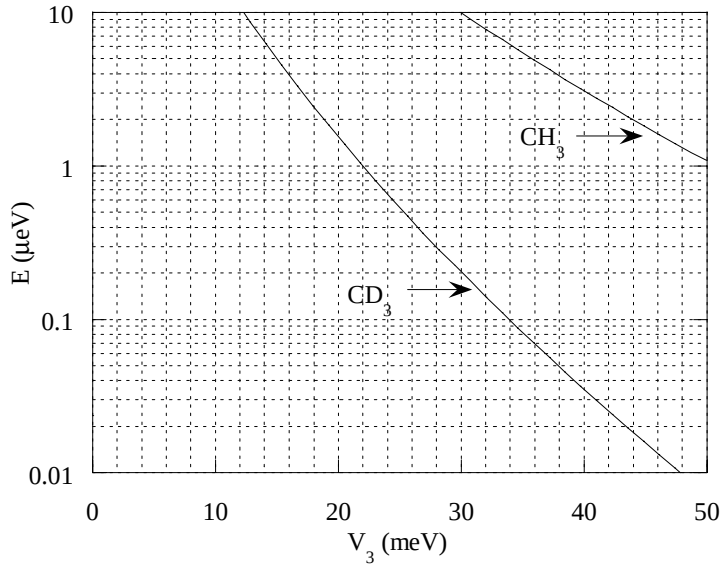


**Figure 6** Potential strength dependence of the one-dimensional rigid rotor $CD_3I$ and $CH_3I$ for the J = 0→1 transition.

As our backscattering measurement proceeds we will be collecting tunneling spectra at a number of different temperatures to see the temperature dependence of the peak positions. As we collect this data we will update a plot of the temperature dependence of the tunnel splitting at the instrument.

Q: *For the current plot displayed at the spectrometer showing the temperature dependence of the tunnel splitting, does this behavior make sense?*

## Appendix A
## Matrix Elements of the 1-D Rigid Rotor in the Three-Fold Potential

The Hamiltonian for the rigid rotor in the three-fold potential is given by equation (6) repeated below

$$H = -\frac{\hbar^2}{2I}\frac{\partial^2}{\partial\phi^2} + V(\phi) \tag{A1}$$

where

$$V(\phi) = \frac{V_3}{2}(1-\cos 3\phi). \tag{A2}$$

The matrix elements can be calculated using the free-rotor basis eigenfunctions

$$\psi_n(\phi) = \frac{1}{\sqrt{2\pi}}\exp(in\phi), \quad n = 0, \pm 1, \pm 2, \ldots \tag{A3}$$

The Hamiltonian (A1) can be decomposed into two parts, $H_{mn} = H^0_{mn} + V_{mn}$, where the elements $H^0_{mn}$ are related to the zero-potential energy levels as

$$H^0_{mn} = \frac{n^2\hbar^2}{2I}\delta_{mn}, \tag{A4}$$

which can be found via the eigenvalue equation for the free rotor Schrödinger equation

$$-\frac{\hbar^2}{2I}\frac{\partial^2}{\partial\phi^2}\psi_n(\phi) = E_n\psi_n(\phi), \tag{A5}$$

with the eigenfunctions given by (A3) and solving for $E_n$. The elements of the potential matrix, $V_{mn}$, are found by calculating the following integral:

$$V_{mn} = \int_0^{2\pi} d\phi\, \psi^*_m(\phi)\frac{V_3}{2}(1-\cos 3\phi)\psi_n(\phi). \tag{A6}$$

Explicit calculation of (A6) and including the zero-potential energy matrix elements (A4) results in the final expression for the matrix elements of the total Hamiltonian:

$$\boxed{H_{mn} = \frac{\hbar^2 n^2}{2I}\delta_{mn} + \frac{V_3}{4}\left\{2\delta_{n,m} - \delta_{n-m+3,0} - \delta_{n-m-3,0}\right\}, \quad n, m = 0, \pm 1, \pm 2, \ldots} \tag{A7}$$

where $\delta_{n,k}$ is the kronecker delta, $\delta_{n,k} = \begin{cases} 1, & n = k \\ 0, & n \neq k \end{cases}$.

The energy eigenvalues shown in figure 3 were found numerically by generating the matrix, $H_{mn}$, for some large number N (we used 41 which gives sufficient accuracy) for a variety of values of $V_3$ and calculating the eigenvalues of $H_{mn}$.

## References


[1]. Squires, G.L. *Introduction to the Theory of Thermal Neutron Scattering* ( Cambridge Unversity Press, Cambridge, London, New York, Melbourne, 1978).

[2]. Prager, M. & Heidemann, A. *Chem.Rev*. **97**, 2933-2966 (1997).

[3]. Horsewill, A.J. *Spectrochimica Acta* **48A**, 379-403 (1992).

[4]. Prager, M., Stanislawski, J. & Hausler, W. *J.Chem.Phys* **86**, 2563-2575 (1987).

## Appendix B
## Relationship Between the Lineshape in Time and Energy

In the section titled *Spectrometer and Data Reduction Details* we stated that the neutrons are recorded as a function of their initial velocity and converted to energy. There is another step in the process necessary to determine the velocity of the neutrons. The counts registered in the neutron detectors are actually recorded as a function of time in fixed width time channels and mapped onto their initial velocities (and then converted to energy transfer via equation (2)). In this appendix we provide a qualitative discussion describing how the raw time-of-flight signal is converted to velocity and energy.

As you have undoubtedly noticed the raw neutron signal displayed on the instrument computer screen (the raw data) is displayed in time-of-arrival at the detectors. As an illustration of such a signal, consider the simulated "raw signal" displayed in figure B.1 composed of two peaks: an elastic peak plus a single inelastic contribution.

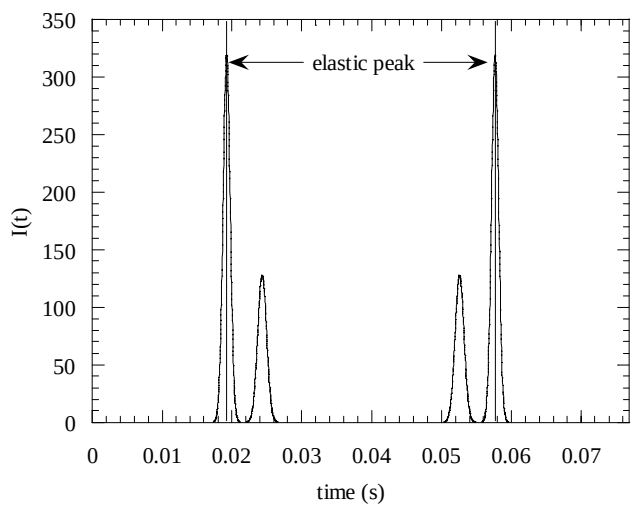


**Figure B.1** Simulated "raw data" collected as a function of time.

The first thing you notice is that there are two sets of two peaks which posess a mirror symmetry about some time (here it is about 38 ms). The reason for this is that the monochromator scans the neutron velocities in two directions over a complete cycle of its motion. Thus the scattering function of the sample is scanned at two different times during one cycle of the monochromator motion. The velocity of the monochromator as a function of time is actually a smoothed triangle function, displayed in figure B.2. Using equation (2) which relates the monochromator velocity to energy transfer one can also plot the energy transfer as a function of time (also displayed in figure B.2).

In figure B.2 note the location in time of the elastic line where v(t) = 0 and E(t) = 0 displayed as vertical lines. These same lines are also shown in the raw time-of-flight signal in figure B.1 as well to illustrate the correspondence between the time and energy. Because of the symmetry of the scan, one lineshape in time is the mirror image of the

other symmetric about ½ the monochromator period ($T_{monochromator}$ = 77 ms in this sample data).

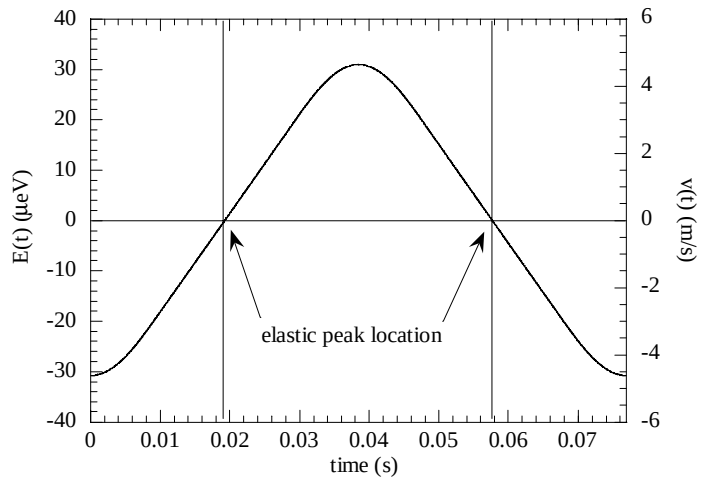


**Figure B.2** Velocity of monochromator and energy transfer to the neutron as a function of time.

The conversion from time to energy consists of three steps: (i) fold the signal in time at the detector about its symmetry point ($T_{sym}$ = 38.5 ms in the example here), (ii) add the resulting signals and, (iii) convert the time axis over ½ the period of the monochromator to energy via equation (2). The result of converting the signal in figure B.1 is shown in figure B.3.

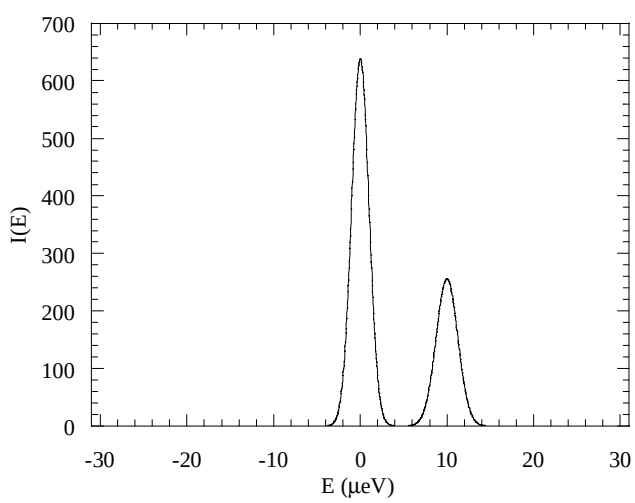


**Figure B.3** Scattering data from figure B.1 after conversion from time to energy.

Q: *The asymmetric lineshape shown in figure B.3 was selected to illustrate the time-to-energy conversion and how the raw lineshape must be folded about some point in time. Does this lineshape seem physically reasonable? (Hint: consider detailed balance and assume that the data shown in this "simulated measurement" were collected at a temperature of 5 K)*

## Appendix C
## Instrument Characteristics for the High Flux Backscattering Spectrometer
## (http://www.ncnr.nist.gov/instruments/hfbs)

Si (111) analyzers covering 20% of $4\pi$ steradians
Si (111) monochromator 52 cm wide × 28 cm tall
$\lambda = 6.27$ Å
$E_f = 2.08$ meV
$v_n = 630$ m/s
16 $^3$He detectors covering $14^o < 2\theta < 121^o$

<u>Dynamic range:</u>

$-32\ \mu eV < \Delta E < 32\ \mu eV$
$0.1\ Å^{-1} < Q_{EL} < 1.7\ Å^{-1}$ (momentum transfer at zero energy transfer)
$\tau \approx 0.1 – 1$ ns

<u>Instrumental resolution:</u>

$\delta E < 1\ \mu eV$ (FWHM)
$\delta Q = 0.1\ Å^{-1} - 0.2\ Å^{-1}$

<u>Flux at sample:</u>

$1.4 \times 10^5$ n/cm$^2$/s

<u>Beam size at sample</u>:

3 cm × 3 cm

<u>Signal to noise:</u>

350:1 for vanadium foil (10% scatterer)

<u>Sample environment</u>:

Furnace (300 K – 1700 K)
Closed cycle refrigerator (30 K – 600 K)
Orange cryostat (1.5 K – 300 K)

## Appendix D
## Effects of the Sample Geometry on Self Shielding and Multiple Scattering

One must consider a number of issues when determining an appropriate sample geometry. A naïve philosophy in designing a sample geometry is to make the sample as big as possible in order to obtain as many scattering events in the shortest possible time. Unfortunately optimization of the experiment is not as simple as this. Sample design involves a careful consideration of the composition of the sample in terms of its scattering and absorption cross-sections.

In an inverse geometry spectrometer like HFBS where the beam passes through the sample twice one must consider *self-shielding* effects which reduce the intensity received at the detectors via absorption. In general absorption in the sample is proportional to the neutron wavelength. On a backscattering spectrometer using Si(111), $E_i$= 2.08 meV, $\lambda$= 6.27 Å, which results in the cross section for absorption being 3.5 times larger than for thermal neutrons with 1.8 Å.

In order to understand the extent to which you have to correct for multiple scattering/self-shielding it is important to know how strong a scatterer/absorber your sample is. The transmission in the forward direction ($2\theta = 0^o$) is often calculated and expressed in terms of a percentage of the incident beam that is scattered/absorbed. For instance, a flat plate sample with total scattering cross-section, $\sigma_{tot} = \sigma_{inc}+\sigma_{coh}$, and absorption cross-section, $\sigma_{abs}$, will have a scattering and absorption determined by

$$\text{scattering} = 1 - \exp\left(-\frac{\mu_s d}{\sin(\pi - 2\theta)}\right) \qquad \text{(flat plate)} \qquad \text{(D1)}$$

$$\text{absorption} = 1 - \exp\left(-\frac{\mu_{abs} d}{\sin(\pi - 2\theta)}\right) \qquad \text{(flat plate)} \qquad \text{(D2)}$$

where $2\theta$ is the angle of orientation of the slab with respect to the incident beam direction, d is the thickness of the slab sample, and $\mu$ is the scattering coefficient (inverse scattering length in $cm^{-1}$) determined by

$$\mu_s = N_A \sigma_{tot} \rho / A \qquad \text{(D3)}$$

$$\mu_{abs} = N_A \sigma_{abs} \rho / A \qquad \text{(D4)}$$

where $N_A$ is Avogadro's number ($6.022 \times 10^{23}$ $mol^{-1}$), $\rho$ is the mass density of the sample material (in g/cc), and A is the molecular weight of the sample in g/mol. On the other hand an annular sample cell has a scattering/absorption in the forward direction determined by

$$\text{scattering} = 1 - \exp(-\pi \mu_s d) \qquad \text{(annular cell)} \qquad \text{(D5)}$$

$$\text{absorption} = 1 - \exp(-\pi\mu_{abs} d) \qquad \text{(annular cell)} \qquad \text{(D6)}$$

where the inverse scattering.absorption lengths are calculated as described above (eqs. D3 and D4) and d is the wall thickness of the annular sample. Equations (D5) and (D6) are good approximations for the cases where $\exp(-\pi\mu d) > 80\%$.

We illustrate the self-shielding corrections for a vanadium sample ($\sigma_{abs}$(1.8 Å) = 5.2 barn) for two different geometries: a flat plate and an annular sample. The intensity in the detectors is very sensitive to the thickness of the sample as well as its geometry. If we assume these two geometries for the same amount of scattering (5%, 10%, and 20% scatterers respectively as calculated via (D1) and (D5)) and assume that the samples are completely illuminated by the incident beam then we obtain the results displayed in figure D.1. The corrected intensity is obtained using $I_{corr}(2\theta,E) = I_{obs}(2\theta,E)/A_{ssc}$ where $I_{obs}(2\theta,E)$ is the observed intensity. It is quite clear that there is a much stronger angle dependence for the correction factor of the slab geometry whereas the corrections are much less for the annular cell. Furthermore, an evaluation of the correction factor is impossible near the orientation angle, $130^o$ in the present example, for the slab geometry. Therefore it is advantageous to use an annular geometry for backscattering.

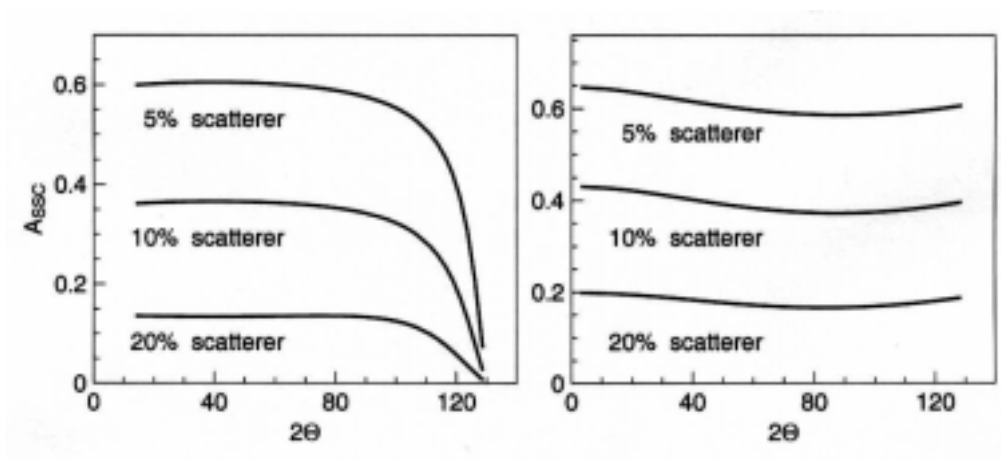


**Figure D.1** Scattering angle dependence of the self-shielding correction factor for (a) flat plate whose normal is oriented $130^o$ with respect to incident beam direction and (b) an annular sample geometry.

When one increases the thickness of the sample for a system with a medium absorption cross-section the intensity will not significantly increase but the effects of multiple scattering will certainly be enhanced. Corrections for multiple scattering are not trivial and, for many systems in which the scattering function is not known a priori, may not be possible at all.

The system shown in figure D.2 illustrates the effects that multiple scattering can have on a system, in this case viscous glycerol. This sample was measured on the IN10 backscattering spectrometer at the ILL at a temperature where the structural relaxation (viscous flow) is on the time scale of the instrument (0.1–1 ns). There is a clear broadening of the lineshape with increasing Q (FWHM ~ $Q^2$) due to the dynamics of the

system. However at Q = 0.19 Å$^{-1}$ structural relaxation cannot be resolved because its too slow at this small Q. The effective broadening in the wings is entirely due to multiple scattering.

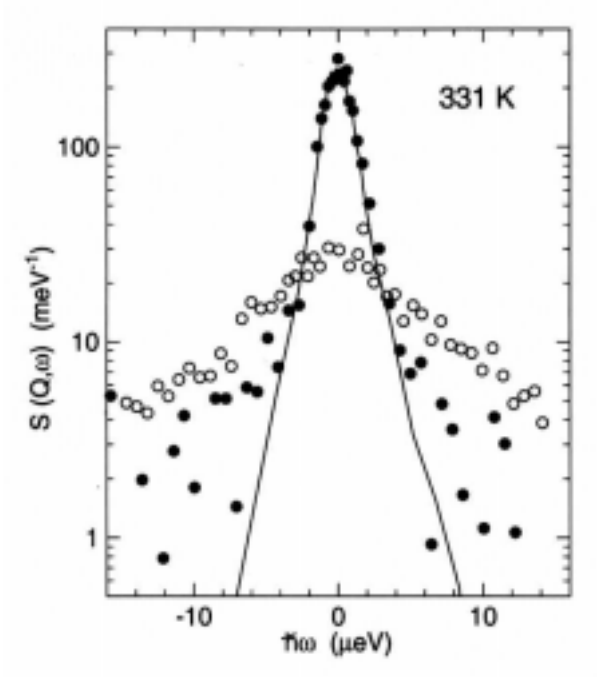


**Figure D.2** Scattering intensity of viscous glycerol taken on the IN10 backscattering spectrometer illustrating the effects of multiple scattering on S(Q,E). Solid line represents the instrumental resolution, open symbols are data taken at Q=1.4 Å$^{-1}$, and the closed symbols are data taken at Q=0.19 Å$^{-1}$ (J. Wuttke et al., Phys. Rev. E **54**, 5364 (1996)).